Available online at www.sciencedirect.com

ScienceDirect

Geochimica et Cosmochimica Acta 279 (2020) 29–44

Geochimica et Cosmochimica Acta

www.elsevier.com/locate/gca

Iron isotope fractionation in hydrous basaltic magmas in deep crustal hot zones

Qi-Wei Li [a,b], Jun-Hong Zhao [b,*], Qiang Wang [a,c,d,*], Zhao-Feng Zhang [a], Ya-Jun An [a], Yu-Ting He [a]

[a] State Key Laboratory of Isotope Geochemistry, Guangzhou Institute of Geochemistry, Chinese Academy of Sciences, Guangzhou 510640, China
[b] State Key Laboratory of Geological Processes and Mineral Resources, School of Earth Sciences, China University of Geosciences, Wuhan 430074, China
[c] CAS Center for Excellence in Tibetan Plateau Earth Sciences, Beijing 100101, China
[d] College of Earth and Planetary Sciences, University of Chinese Academy of Sciences, Beijing 100049, China

Received 12 September 2019; accepted in revised form 21 March 2020; Available online 6 April 2020

Abstract

Mafic magmatism within deep crustal hot zones plays an important role in the crustal formation and evolution. High-pressure garnet crystallization drives magma differentiation and Fe isotope fractionation at the base of the lower crust. The ~840 Ma intrusion and the associated ~830 Ma dikes from the Tongde region in South China consist mainly of gabbro and diorite, which record complicated magmatic processes of the deep crustal zones and provide new insights into the Fe isotope fractionation. Rocks from the Tongde intrusion have high Sr/Y ratios (61–163) and variable δ^{57}Fe values (+0.07 to +0.21‰ relative to IRMM-014) that initially increase then decrease with progressive magmatic differentiation. All samples do not display obvious imprint of deuteric fluid exsolution, and residual garnet in the mantle source did not fractionate the Fe isotope compositions of the primary magmas significantly. The variable Fe isotope signatures in this study can be reproduced by sequential fractional crystallization of olivine/pyroxene and garnet in the deep crust followed by amphibole saturation in the upper section. The host rocks of the intrusion underwent diffusive exchange with the dikes. Removal of both isotopically light- and heavy-Fe minerals well explains the small Fe isotope fractionation in mafic and intermediate rocks. The high-Sr/Y suites of the intrusion and dikes have an average δ^{57}Fe of +0.11 ± 0.02‰ (2SD), similar to the value of arc crust at convergent continental margins. Therefore, garnet fractionation is an important process in arc roots, which drives the melts evolving to calc-alkaline series. Fractional crystallization of hydrous basaltic magmas under high pressures in deep crustal hot zones makes a significant contribution to the formation and evolution of continental crust.

Keywords: Fe isotopes; Fractional crystallization; Garnet; Deep crustal hot zones

1. INTRODUCTION

Deep crustal hot zones are major sites of crustal formation and evolution at active continental margins, with mafic magmas providing essential materials for crustal growth and heat for melting surrounding crustal rocks (Annen et al., 2006; Solano et al., 2012; Klaver et al., 2018). Garnet is a key mineral during magma emplacement at the base of the lower crust, and its fractionation drives the melts evolving to high Sr/Y rocks (Green, 1972; Müntener and Ulmer, 2006; Alonso-Perez et al., 2009). Intermediate to silicic adakites have been extensively studied (Defant and

* Corresponding authors.
E-mail addresses: jhzhao@cug.edu.cn (J.-H. Zhao), wqiang@gig.ac.cn (Q. Wang).

https://doi.org/10.1016/j.gca.2020.03.032
0016-7037/

Drummond, 1990), and are considered to have been produced by partial melting of source rocks in equilibrium with garnet and amphibole (Moyen, 2009) or high-pressure fractionation of hydrous magmas (Macpherson et al., 2006; Kolb et al., 2012). These processes are hard to be distinguished through whole-rock elements and radiogenic isotopes that can be easily changed by mineral accumulation and variable melt interaction with mantle and crust (Castillo, 2012; Ribeiro et al., 2016), but may imprint on Fe isotopes (He et al., 2017). Therefore, Fe isotopes of arc-affinity igneous rocks, especially for high-Sr/Y mafic rocks, are crucial for clarifying the role of garnet in basaltic magma evolution and formation of lower arc crust (e.g., Alonso-Perez et al., 2009; Chiaradia et al., 2009), but rarely have been reported.

Fe is a major polyvalent element in silicate melts, and the relative proportions of ferrous and ferric iron controlled by magmatic oxygen fugacity (fO_2), ensue iron isotope fractionation with physical addition or removal of Fe (Nebel et al., 2015; Sossi et al., 2016). Fe^{3+}, which has high charge, low coordination number and short bond length, displays larger bond strength and higher force constant than Fe^{2+} (Sossi et al., 2016). Synchrotron method of Nuclear Resonant Inelastic X-ray Scattering (NRIXS) measurement reveals that the equilibrium isotope fractionation factor is proportional to the force constant at a given temperature, leading to heavy iron isotopes being preferentially partitioned into Fe^{3+}-bearing phases (Dauphas et al., 2014). Therefore, melts are generally heavier in Fe isotopes than their protolith and minerals due to the incompatibility of Fe^{3+} during partial melting and fractional crystallization (Canil et al., 1994; Weyer, 2008; Dauphas et al., 2014). However, magnetite crystallization under oxidized conditions would lower Fe isotopes of the melts (Polyakov et al., 2007). Kinetic fractionation of thermal (Soret) and chemical diffusion can generate extreme Fe isotope compositions (Huang et al., 2009; Richter et al., 2009; Teng et al., 2011; Wu et al., 2018).

Heavy δ^{57}Fe values are widely recognized in high-Si granitic rocks and are interpreted as results of deuteric fluid exsolution (Poitrasson and Freydier, 2005; Heimann et al., 2008), delayed magnetite saturation (Foden et al., 2015), or removal of Fe^{2+}-bearing minerals (Schuessler et al., 2009; Sossi et al., 2012; Dauphas et al., 2014; Du et al., 2017). However, basaltic and andesitic rocks exhibit homogeneous Fe isotope compositions with δ^{57}Fe variations less than three tenths of permil (Poitrasson and Freydier, 2005; Heimann et al., 2008; Schuessler et al., 2009; Sossi et al., 2012; Telus et al., 2012; Zambardi et al., 2014; Foden et al., 2015; Gajos et al., 2016; Du et al., 2017; He et al., 2017; Wu et al., 2017; Xia et al., 2017). Many models have been proposed to explain the small Fe isotope fractionation, such as Fe fractions in mafic melts being too high to be affected, undersaturation of magnetite preventing its early crystallization, high magmatic temperatures resulting in low fractionation factors, and co-precipitation of Fe^{2+}- and Fe^{3+}-bearing phases under different fO_2 conditions (Heimann et al., 2008; Schuessler et al., 2009; Li et al., 2019). The island arc lavas have been extensively studied and are suggested to have light Fe isotope compositions due to early melt extraction and metasomatism in the mantle wedge (Dauphas et al., 2009; Nebel et al., 2015; Foden et al., 2018). Although their Fe isotope fractionation induced by olivine and pyroxene fractionation and magnetite saturation has been well addressed (e.g., Nebel et al., 2015; Williams et al., 2018), the effects of garnet and amphibole fractionation on Fe isotopes in deep crustal hot zones, as well as their contributions for the calc-alkaline magma evolution at convergent margins are largely unknown.

The Neoproterozoic Tongde intrusion, located at western margin of the Yangtze Block in South China, was cut by numerous post-magmatic mafic dikes; both the intrusion and dikes were formed in a continental arc setting (Li and Zhao, 2018). In this paper, we systematically studied whole-rock Fe isotopes of the gabbroic and dioritic samples from the intrusion to constrain magmatism in the lower crust, and the equilibrium and kinetic process effects on Fe isotope fractionation. Our results indicate that Dy/Yb ratios and δ^{57}Fe values increase then decrease with progressive magmatic differentiation that are inconsistent with deuteric fluid exsolution or residual garnet in the source. Instead, sequential fractional crystallization of olivine/pyroxene and garnet in the deep crust followed by amphibole saturation in the upper section well explains the elemental and Fe isotopic variations. The host rocks of the intrusion underwent diffusive exchange with the dikes indicated by some light δ^{57}Fe samples (down to −0.08‰) in the latter. Removal of both isotopically light- and heavy-Fe minerals may result in the homogeneous Fe isotope compositions in basaltic and andesitic rocks. The high-Sr/Y rocks of the intrusion and dikes have an average δ^{57}Fe value similar to that of arc crust at convergent continental margins, suggesting that garnet fractionation in deep crustal hot zones is an important process for the evolution of calc-alkaline magmas and formation of continental crust.

2. BACKGROUND AND SAMPLE DESCRIPTION

Samples were collected from the *ca.* 840 Ma intrusion that was cut by numerous *ca.* 830 Ma dikes in the Tongde region at the western margin of the Yangtze Block in South China (Figs. 1 and 2a; Sun, 2009; Li and Zhao, 2018). The intrusion is an ellipsoidal body which covers an area of ~300 km^2 and consists of gabbro and diorite. The gabbros are fine-grained and locally occur as irregular and ductile stretched enclaves in the main medium-grained diorites (Fig. 2b). The gabbros are composed of subhedral plagioclase (~50 vol.%), subhedral-anhedral clinopyroxene (10–20 vol.%) and orthopyroxene (15–20 vol.%) associated with minor anhedral amphibole (5–15 vol.%) (Fig. 2c). The diorites mainly consist of subhedral plagioclase (45–55 vol.%) and subhedral-anhedral amphibole (20–40 vol.%), as well as less amounts of subhedral-anhedral clinopyroxene (<7 vol.%) and orthopyroxene (<13 vol.%) (Fig. 2d). Fine-grained accessory minerals, such as magnetite, ilmenite, pyrite, titanite, apatite and zircon, are sporadically observed in the samples (Table S1; Sun, 2009). Both the gabbro and diorite show low to medium SiO_2 (46.10–56.90 wt.%), MgO (2.74–7.00 wt.%) and FeO_t contents

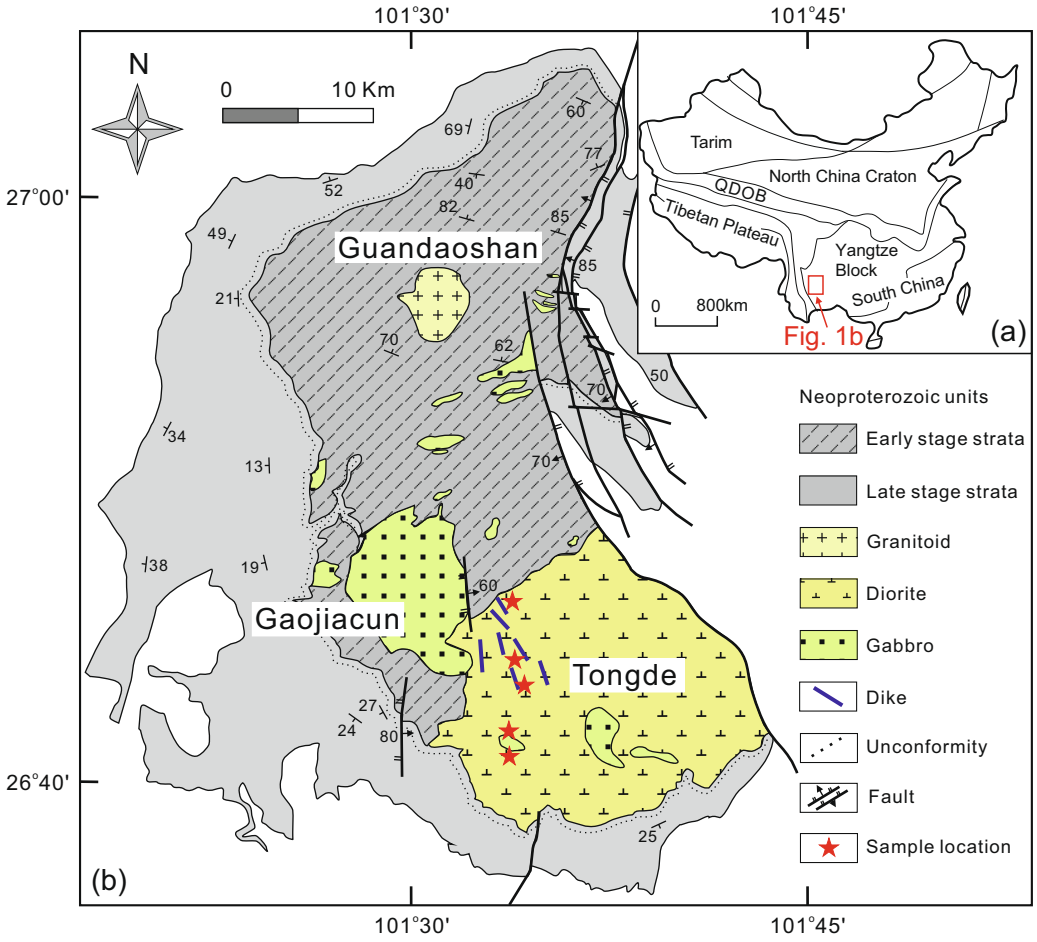

Fig. 1. Simplified geological map showing the major units in China (a) and distributions of the Tongde intrusion and dikes at the western margin of the Yangtze Block (b; modified from Li and Zhao, 2018).

(5.65–10.59 wt.%), high Sr/Y (61–163) and Dy/Yb ratios (2.2–3.0), as well as constant initial $^{87}Sr/^{86}Sr$ ratios (0.7051–0.7053) and εNd(t) values (+0.9 to +1.5) (Table S2). They underwent minor or negligible crustal contamination and show arc-like elemental signatures that characterized by enrichment of large-ion lithophile elements and depletion of high-field-strength elements, and were considered to have been generated by partial melting of a garnet lherzolite mantle source (Sun, 2009).

The dikes are 0.5–4.0 m wide and ~1 km long, and consist of fine- to medium-grained diorite that is composed of subhedral-anhedral amphibole (30–75 vol.%) and plagioclase (25–60 vol.%), with minor magnetite and apatite (Fig. 2e-f). They display variable SiO_2 (49.81–59.90 wt.%), MgO (1.99–11.67 wt.%) and FeO_t contents (5.38–11.22 wt.%), Sr/Y (12–115) and Dy/Yb ratios (1.7–2.7). Their initial $^{87}Sr/^{86}Sr$ ratios (0.7049–0.7063) and εNd(t) values (+0.6 to +2.0) are similar to those of the host intrusion (Table S2). These rocks were formed by high-pressure fractional crystallization of hydrous basaltic magmas with minor amphibole accumulation (Li and Zhao, 2018).

3. ANALYTICAL METHODS

Approximately 20 mg of sample powder was digested in a concentrated HF-HNO_3 (3:1) mixture on a hotplate at 120 °C. ~200 μg Fe was loaded on the AG1-X8 (200–400 mesh) anion exchange column after evaporation and chemical equilibrium by adding 0.5 ml of 6 N HCl. Total procedural blank for Fe was 25 ng and negligible compared to the large amount of Fe loaded on the column. The recovery of the procedure was >99%. Iron isotope measurements were carried out on a Nu Plasma 1700 multi-collector inductively coupled plasma mass spectrometer (MC-ICP-MS) in the State Key Laboratory of Isotope Geochemistry at the Guangzhou Institute of Geochemistry, Chinese Academy of Sciences. Isotopic ratios were determined by the sample-standard bracketing method at a pseudo-high resolution mode with resolving power of 15000. Concentrations of samples were adjusted to the standard with 2 ppm Fe to correct instrumental drift and mass bias, resulting in ~12 V intensity on ^{56}Fe. Each sample was measured for at least three times and the weighted average was taken as the iron isotope ratio. Fe isotope data are reported relative to

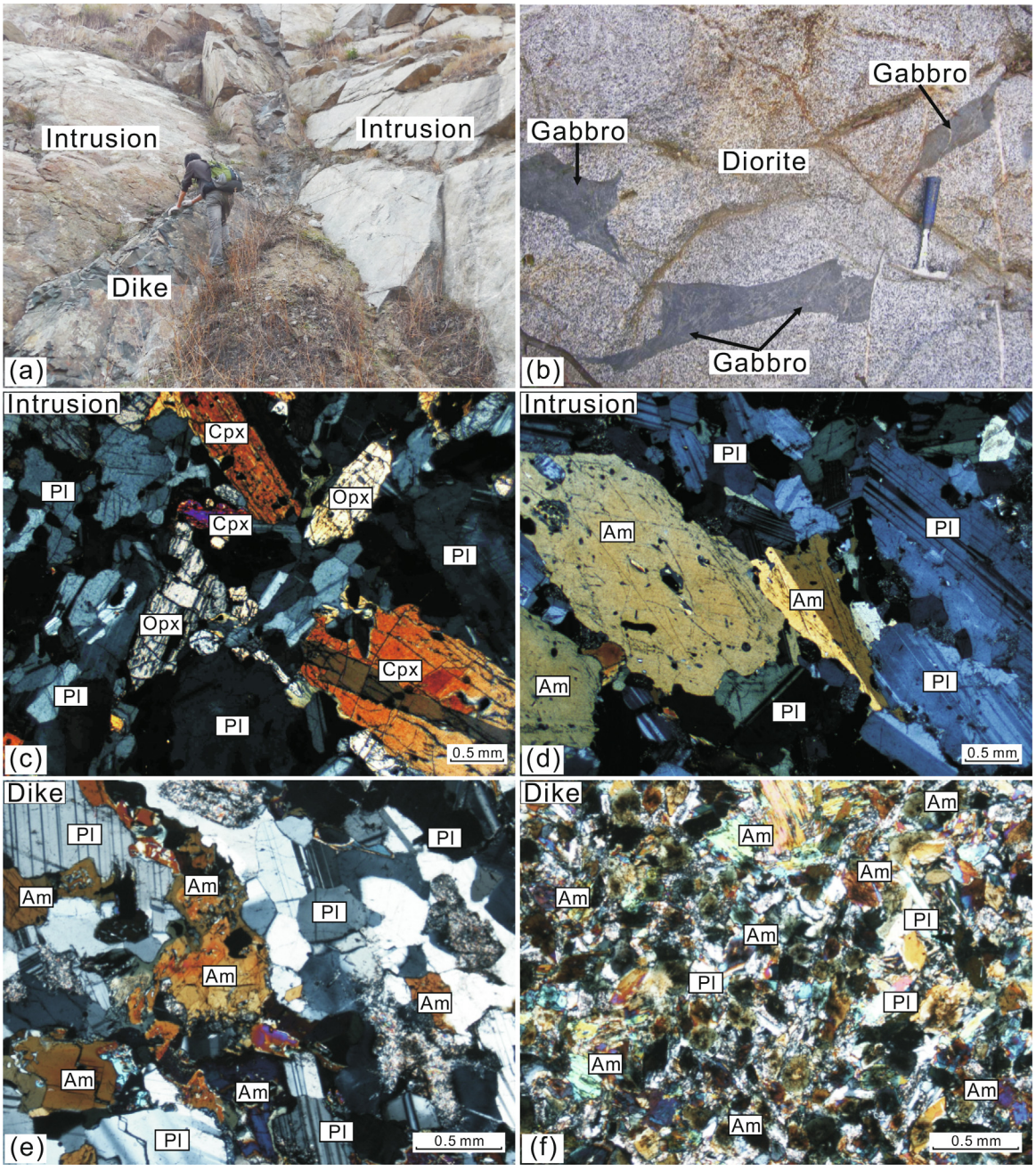

Fig. 2. (a) The dikes emplaced into the intrusion (Li and Zhao, 2018); (b) The gabbro and diorite of the Tongde intrusion (Sun, 2009); Representative photomicrographs showing typical textures of gabbro and diorite from the Tongde intrusion (c-d) and diorite from the dikes (e-f).

the IRMM-014 standard in the delta notation: $\delta^{57(56)}Fe = {}^{57(56)}Fe_{sample}/{}^{54}Fe_{sample}/{}^{57(56)}Fe/{}^{54}Fe_{IRMM-014} - 1) \times 1000$. Long-term external reproducibility is ± 0.05‰ for δ^{56}Fe based on replicate analyses of reference materials. The measured Fe isotope compositions of the international standard BHVO-2 have an average of δ^{56}Fe (+0.12 ± 0.04‰, 2SD) and δ^{57}Fe (+0.21 ± 0.07‰, 2SD) (n = 6), in agreement with the recommended values within analytical uncertainties (Craddock and Dauphas, 2011; He et al., 2015). Duplicate analyses indicated good reproducibility (Table 1). Detailed Fe purification and analytical procedures are described by Zhang et al. (2019).

4. RESULTS

Fe isotope compositions for samples from the Tongde intrusion are presented in Table 1. Their δ^{57}Fe values range from +0.07 ± 0.05‰ to +0.21 ± 0.04‰ with a weighted

Table 1
Iron isotope compositions of the Tongde intrusion, South China.

Sample	$\delta^{56}Fe$	±2SD	$\delta^{57}Fe$	±2SD	$\delta^{57}Fe$ prim	MgO* (wt.%)	Fe_2O_3* (wt.%)	n[a]
TD1	+0.09	0.05	+0.16	0.09	+0.13	4.64	8.64	5
TD5	+0.11	0.02	+0.17	0.07	+0.13	4.45	8.44	3
TD8	+0.09	0.04	+0.12	0.05	+0.09	4.13	8.20	3
TD9	+0.13	0.03	+0.19	0.04	+0.16	4.48	8.22	3
TD10	+0.12	0.06	+0.15	0.14	+0.12	4.37	8.05	3
TD11	+0.09	0.03	+0.12	0.05	+0.09	4.20	8.18	4
TD13	+0.13	0.03	+0.19	0.08	+0.16	4.32	8.20	3
TD16	+0.09	0.02	+0.14	0.09	+0.11	4.12	8.48	3
TD18	+0.12	0.04	+0.21	0.04	+0.17	5.01	9.82	3
TD24	+0.04	0.05	+0.07	0.07	+0.06	6.57	7.02	3
TD25	+0.09	0.02	+0.13	0.02	+0.08	2.74	9.15	3
TD25R[b]	+0.10	0.02	+0.16	0.05	+0.11	2.74	9.15	3
TD28	+0.09	0.04	+0.14	0.07	+0.11	5.43	9.11	4
TD36	+0.07	0.01	+0.11	0.05	+0.09	7.00	11.77	3
TD40	+0.06	0.05	+0.07	0.05	+0.04	4.89	9.02	3
TD42	+0.09	0.02	+0.16	0.07	+0.13	5.44	9.72	3
TD45	+0.06	0.04	+0.12	0.11	+0.08	2.99	6.28	4
TD50	+0.10	0.05	+0.17	0.11	+0.15	4.83	8.40	4
BHVO-2	+0.12	0.04	+0.21	0.07				6

[a] n denotes the total number of analyses per newly purified sample solution by MC-ICPMS.
[b] R denotes the repeat sample dissolution, column chemistry and instrumental analysis.
* Data taken from Sun (2009).

mean of +0.14 ± 0.02‰ (2SD, n = 17), similar to those of mafic and intermediate rocks worldwide (+0.05 to +0.25‰; Poitrasson and Freydier, 2005; Heimann et al., 2008; Teng et al., 2008; Dauphas et al., 2009; Schuessler et al., 2009; Sossi et al., 2012; Telus et al., 2012; He et al., 2017). Rocks from the intrusion display similar whole-rock elemental and Sr-Nd-Fe isotopic data to those of the dikes (Fig. 3; Li and Zhao, 2018). No apparent correlations have been observed for $\delta^{57}Fe$ against Sr and Nd isotopes (Fig. 3).

5. DISCUSSION

The mafic and intermediate rocks are generally formed by fractional crystallization of basaltic magmas or mafic mineral accumulation in the more evolved melts (Jagoutz et al., 2007; Xu et al., 2019). Cumulate textures are characterized by medium- to coarse-grained, euhedral pyroxene and amphibole associated with interstitial plagioclase. Cumulate rocks generally show largely variable major and trace elements and Fe isotopes, but constant Sr-Nd isotopes similar to their primary melts (e.g., Schoenberg et al., 2009; Xu et al., 2019). In contrast, non-cumulate gabbro-diorites are fine- to medium-grained and show gabbroic or equigranular textures, in which pyroxene, amphibole and plagioclase are mostly subhedral, and thus represent frozen liquids with minor or negligible crystal accumulation (Zhao and Asimow, 2018; Xu et al., 2019). Rocks from the Tongde intrusion consist of subhedral pyroxene, amphibole and plagioclase (Fig. 2c and d; Table S1). They show variable SiO_2 (46.10–56.90 wt.%) that is negatively correlated with MgO, Al_2O_3, FeO_t and CaO (Fig. S1). All samples display right-inclined chondrite-normalized rare earth element (REE) patterns and lack middle REE enrichment (Fig. 4), ruling out significant amphibole accumulation (Tiepolo et al., 2007). Calculations reveal that Mg# values of the melts in equilibrium with the most primitive clinopyroxene (Mg# = 71–75; Table S3) are 47–52 using an Fe-Mg exchange coefficient of 0.36 between clinopyroxene and equilibrated melts (e.g., Gaetani et al., 2003; Putirka, 2008; Dalou et al., 2012), similar to their whole-rock Mg# values (51–52; Table S2). These lines of evidence suggest that rocks from the Tongde intrusion were formed by fractional crystallization following the liquid line of descent, and thus can be used to trace the magma evolution.

5.1. Effects of fluid exsolution on Fe isotope fractionation

Primary basaltic magmas in arc settings are estimated to have H_2O contents of 2–6 wt.% based on the observations of nature samples, melt inclusions, experimental phase equilibrium and thermodynamic calculations (Anderson, 1979; Sisson and Grove, 1993; Carmichael, 2002, 2004; Cervantes and Wallace, 2003; Grove et al., 2003; Barclay and Carmichael, 2004). Differentiated melts are expected to be rich in H_2O due to decompression induced by magma ascent and decreasing solubility of volatiles (Baker and Alletti, 2012). Fluid bubbles break up at high crustal levels, result in separation between fluids and melts in the later stage of magma evolution (Candela, 1986). The Tongde intrusion was formed at the active western margin of the Yangtze Block during the Neoproterozoic (Zhao et al., 2011, 2018). Aqueous fluid exsolution should be firstly addressed in discussing the Fe isotope budget of the melts.

Iron is readily partitioned into aqueous phases and forms ferrous iron- and halogen-rich complexes (Chou and Eugster, 1977; Simon et al., 2004), their removal makes the residual melts to be rich in heavy Fe isotopes

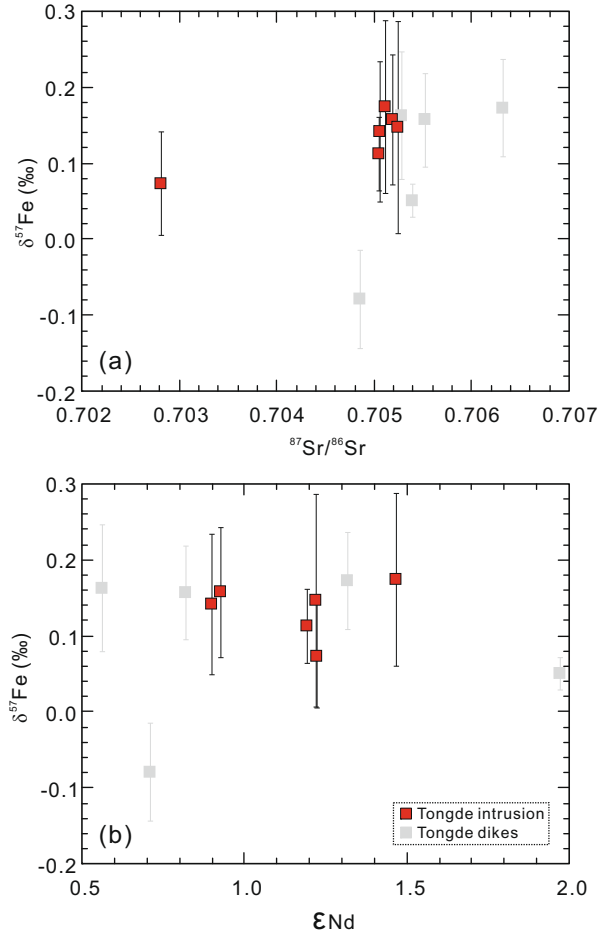

Fig. 3. Plots of $^{87}Sr/^{86}Sr$ and εNd against $\delta^{57}Fe$ for rocks from the Tongde intrusion and dikes. Error bar denotes two standard deviations (2SD). Whole-rock Sr and Nd isotope data of the intrusion and dikes are from Sun (2009) and Li and Zhao (2018), and Fe isotope data of the dikes from Li et al. (2020).

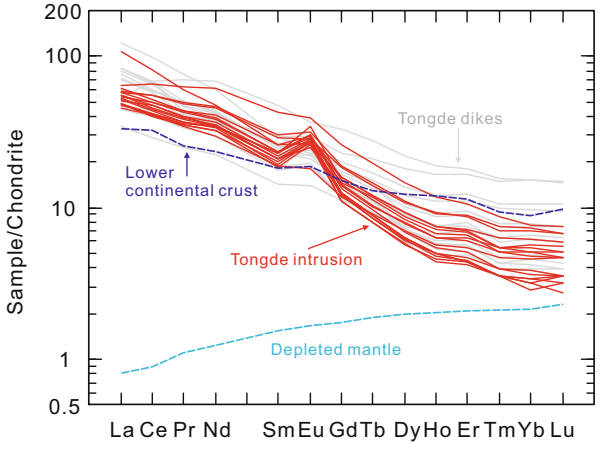

Fig. 4. Chondrite-normalized REE patterns for rocks from the Tongde intrusion and dikes. The lower continental crust (Rudnick and Gao, 2003) and depleted mantle (Workman and Hart, 2005) are shown for comparison.

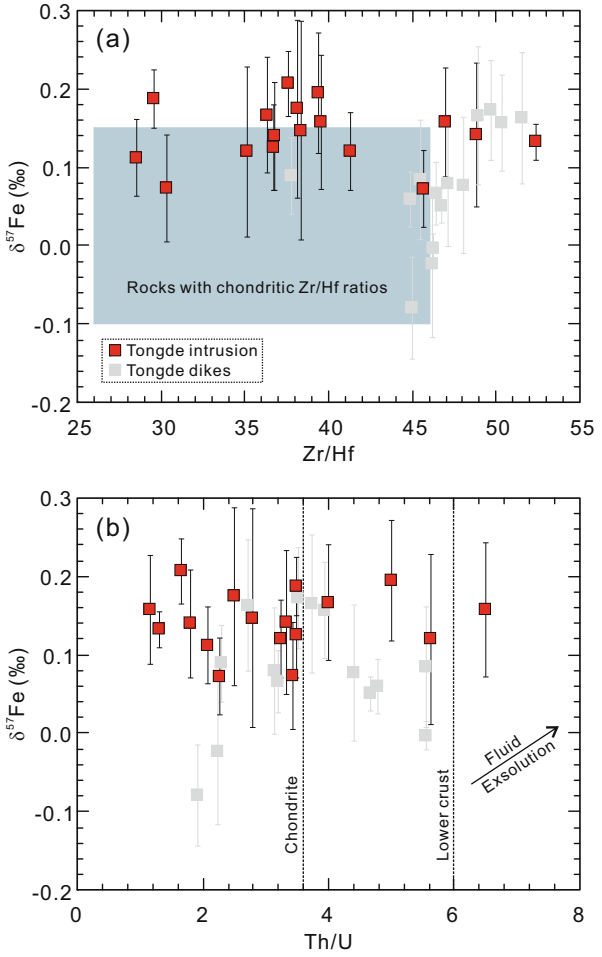

Fig. 5. Plots of Zr/Hf and Th/U against $\delta^{57}Fe$ for rocks from the Tongde intrusion and dikes. The field of rocks with chondritic Zr/Hf ratios is from Heimann et al. (2008).

(Poitrasson and Freydier, 2005; Heimann et al., 2008). Zr/Hf could be reduced (lower than 26) and Th/U ratios increased (higher than 10) during fluid-magma interactions due to higher mobilities of Zr and U over Hf and Th in fluids (Bau, 1996; Hawkesworth et al., 1997), although both ratios remain near-chondritic values in magmatic processes (e.g., partial melting and fractional crystallization). Rocks from the Tongde intrusion have high Zr/Hf (29–52) and low Th/U ratios (1.2–6.5) that are not correlated with $\delta^{57}Fe$ values (Fig. 5), suggesting that fluid exsolution did not fractionate Fe isotopes.

5.2. Minor role of residual garnet in Fe isotope fractionation

High Sr/Y mafic and intermediate rocks are generally produced by partial melting of a garnet-bearing mantle source, or by high-pressure fractional crystallization of hydrous basaltic magmas (Hoffer et al., 2008; Chiaradia et al., 2009; Li and Zhao, 2018). It is therefore necessary to distinguish these two processes and clarify their contributions to Fe isotope variations. Samples from the Tongde

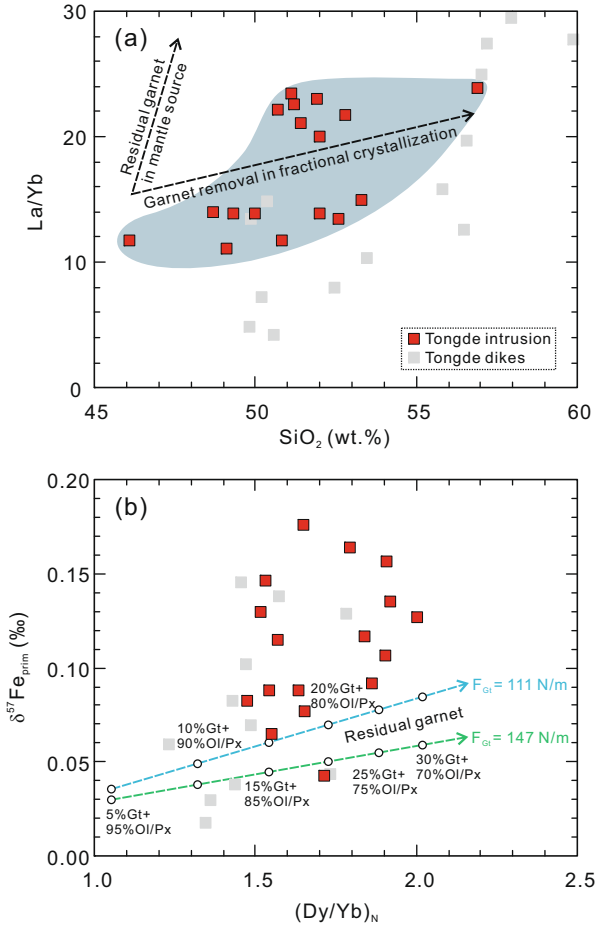

Fig. 6. Plots of La/Yb vs. SiO_2 and $\delta^{57}Fe_{prim}$ vs. $(Dy/Yb)_N$ for rocks from the Tongde intrusion and dikes. The primary melts derived from the garnet-bearing mantle source have low SiO_2 contents of 44–47 wt.% (Walter, 1998) and high La/Yb ratios. Rocks from the Tongde intrusion show variable La/Yb and SiO_2 and follow the garnet fractionation trend (Macpherson et al., 2006). The parameters used in calculations are listed in Table 3.

intrusion show high Sr/Y (61–163) and $(La/Yb)_N$ ratios (8–17) (Table S2; Fig. 4), which are positively correlated with SiO_2, deviating from the partial melting trends with residual garnet in the source (Fig. 6a). The batch melting model was used to determine melt compositions and petrogenesis from a depleted garnet lherzolite mantle source (Shaw, 1970). Considering the key role of garnet in controlling Fe isotopes of the melts, two garnet Fe-O force constants (111 and 147 N/m calculated with ionicity of 0.47 and 0.36, respectively) were used to estimate possible Fe isotope variations during partial melting (Sossi and O'Neill, 2017). Olivine and pyroxene have average force constant of 196 N/m (Jackson et al., 2009; Dauphas et al., 2014). Force constant of basaltic melts is supposed to be 230 N/m based on its positive correlation with $Fe^{3+}/\sum Fe$ ratios (Dauphas et al., 2014) using an oxygen fugacity of FMQ + 1 (Evans et al., 2012). The fractionation factor between mineral and melt is calculated by:

$$\Delta^{57}Fe_{mineral-melt} = 4284 \times \frac{[F_{mineral} - F_{melt}]}{T^2} \quad (1)$$

where F is the force constant and T is temperature in Kelvin (Sossi and O'Neill, 2017). The melt has $\delta^{57}Fe$ values of:

$$\delta^{57}Fe_{melt} = \Delta^{57}Fe_{melt-residue} + \delta^{57}Fe_{residue} \quad (2)$$

Fe isotope fractionation between residue and protolith is negligible at low degrees of partial melting (<0.02‰ with 20% melting; Dauphas et al., 2009). Thus, Eq. (2) can be written as:

$$\delta^{57}Fe_{melt} = \Delta^{57}Fe_{melt-residue} + \delta^{57}Fe_{protolith} \quad (3)$$

where $\Delta^{57}Fe_{melt\text{-}residue}$ is calculated using Eq. (4) (He et al., 2017):

$$\Delta^{57}Fe_{melt-residue} = \Delta^{57}Fe_{melt-ol/px} - \frac{D_{Fe} \times V_{gt}}{V_{ol/px} + D_{Fe} \times V_{gt}} \times \Delta^{57}Fe_{gt-ol/px} \quad (4)$$

Melt Fe-isotope compositions are acquired through a combination of Eqs. (3) and (4):

$$\delta^{57}Fe_{melt} = \Delta^{57}Fe_{melt-ol/px} - \frac{D_{Fe} \times V_{gt}}{V_{ol/px} + D_{Fe} \times V_{gt}} \times \Delta^{57}Fe_{gt-ol/px} + \delta^{57}Fe_{protolith} \quad (5)$$

where D_{Fe} is partition coefficient of Fe between garnet and olivine/pyroxene. V_{gt} and $V_{ol/px}$ are proportions of garnet (gt) and olivine/pyroxene (ol/px) in the residue, respectively. Assume that mantle melting occurred at 1400 °C, Fe isotope fractionation factors are $\Delta^{57}Fe_{gt\text{-}ol/px} = -0.13‰$ or −0.07‰ and $\Delta^{57}Fe_{melt\text{-}ol/px} = +0.05‰$ (Table 2), which are in the reported range (e.g., Beard and Johnson, 2004; Williams et al., 2009; Sossi et al., 2012; An et al., 2017). $\delta^{57}Fe$ value of the depleted sub-arc mantle is supposed to be −0.03‰ (Table 3; Weyer and Ionov, 2007; Sossi et al., 2016). Our calculations indicate that both $(Dy/Yb)_N$ (1.05–2.01) and $\delta^{57}Fe$ (+0.04 to +0.08‰ and +0.03 to

Table 2
Force constants and fractionation factors used in the modeling.

Phase	Force constant (N/m)	$\Delta^{57}Fe$ (‰)
Partial melting (T = 1400 °C)		
Ol/Px	196	
Gt (I = 0.47)	111	
Gt (I = 0.36)	147	
Melt	230	
Gt-Ol/Px (I = 0.47)	−85	−0.13
Gt-Ol/Px (I = 0.36)	−49	−0.07
Melt-Ol/Px	34	+0.05
Fractional crystallization (T = 1150 °C)		
Ol/Px	196	
Gt (I = 0.47)	111	
Gt (I = 0.36)	147	
Am	250	
Melt	230	
Ol/Px-Melt	−34	−0.07
Gt-Melt (I = 0.47)	−119	−0.25
Gt-Melt (I = 0.36)	−83	−0.18
Am-Melt	20	+0.04

Abbreviations: Ol, olivine; Px, pyroxene; Gt, garnet; Am, amphibole; I, ionicity.

Table 3
Modeling parameters for garnet lherzolite partial melting.

		FeO (wt.%)	δ^{57}Fe (‰)	Dy (ppm)	Yb (ppm)
	Source composition	8.18	−0.03	0.51	0.37
Partition coefficient	Gt	$D_{Gt/Ol}$ $_{(Px)} = 2.17$		4.4	14
	Ol/Px			1.2	0.9
Predicted melts for < 10% melting of garnet lherzolite at 1400 °C					
Source mineralogy					
Gt	Ol/Px		$(Dy/Yb)_N$	$\delta^{57}Fe_{melt}$ (‰) ($F_{Gt} = 111$ N/m)	$\delta^{57}Fe_{melt}$ (‰) ($F_{Gt} = 147$ N/m)
0.05	0.95		1.05	0.035	0.030
0.10	0.90		1.32	0.047	0.037
0.15	0.85		1.54	0.058	0.043
0.20	0.80		1.72	0.068	0.048
0.25	0.75		1.88	0.077	0.054
0.30	0.70		2.01	0.085	0.058

Partition coefficients for Gt and Ol/Px are from He et al. (2017). The source compositions of garnet lherzolite are from Workman and Hart (2005) and Weyer and Ionov (2007).

+0.06‰ using garnet force constants of 111 and 147 N/m, respectively) increase in the melts with 5–30% residual garnet in the source region (Fig. 6b).

If rocks from the Tongde intrusion were derived from a garnet-bearing mantle source and experienced fractional crystallization of olivine and pyroxene, it is necessary to correct Fe isotope compositions for the effects of mineral fractionation using the method of Sossi et al. (2016). The primary basaltic melts are supposed to have Mg# value of 74 that is chemically in equilibrium with peridotite with Mg# of 90 (Sossi et al., 2016; Nebel et al., 2018). The mineral-melt fractionation factor of $\Delta^{57}Fe_{mineral\text{-}melt} \times 10^6/T^2 = -0.15$ is derived by Fe-O force constants (Table 2), and the starting $Fe^{3+}/\sum Fe$ is 0.2 (Evans et al., 2012). Dy/Yb ratios are not significantly varied due to their low partition coefficients in olivine and pyroxene. Results show that the Fe isotope compositions of the primary melts ($\delta^{57}Fe_{prim}$) range from +0.04‰ to +0.17‰ (Table 1), which are much heavier than those of the modeled melts at the same proportions of residual garnet (Fig. 6b), suggesting limited effects of residual garnet on Fe isotope fractionation during partial melting of the mantle source.

5.3. Fractional crystallization in deep crustal hot zones

Calc-alkaline magmas generally have high water contents and fO_2 which are inherited from mantle wedges modified by slab-derived materials (Kelley and Cottrell, 2009; Zimmer et al., 2010; Chin et al., 2018). Repeated magma underplating/intruding, high-pressure fractional crystallization, and melt-rock interaction in deep crustal hot zones significantly modify structures and chemical compositions of the lower arc crust (Annen et al., 2006). Garnet is stable in hydrous basaltic and andesitic melts under high pressures (0.8–1.2 GPa) and temperatures (800–1000 °C), corresponding to conditions of arc roots at convergent continental margins (Alonso-Perez et al., 2009). Amphibole is also an important mineral, which is controlled by magmatic H_2O contents in hydrous calc-alkaline melts and crystallizes under the conditions of 8 wt.% H_2O at 1000 °C to 4 wt.% H_2O at 850 °C (Davidson et al., 2007; Alonso-Perez et al., 2009; Dessimoz et al., 2012).

Rocks from the Tongde intrusion record magma evolution in a deep crustal hot zone (Sun, 2009; Li and Zhao, 2018). Their high Sr/Y (61–163) and $(La/Yb)_N$ ratios (8–17) indicate that the melts were in equilibrium with garnet and/or amphibole. Amphibole has higher partition coefficients for middle REE (relative to heavy REE) than garnet, implying that Dy/Yb ratio is effective to distinguish fractionated phases. Furthermore, garnet has lower Fe-O force constant and mineral-melt Fe isotope fractionation factor than amphibole (Sossi and O'Neill, 2017; Ye et al., 2020), and thus garnet fractionation will elevate, whereas amphibole removal may lower δ^{57}Fe values of the melts.

Rhyolite-MELTS calculations reveal that pyroxene, garnet and amphibole crystallized at 1120 °C, 1010 °C and 940 °C, respectively, in the basaltic liquids of the Tongde intrusion (Fig. S2; Gualda et al., 2012). These samples show two stages of variations in Dy/Yb ratios and δ^{57}Fe values in plots against indices of magmatic differentiation, with an initially sharp increase and then decrease with increasing SiO_2 and decreasing MgO contents (Fig. 7a–d). The mafic samples ($SiO_2 < 48$ wt.%) exhibit constant Dy/Yb ratios and slightly increasing δ^{57}Fe values (Fig. 7a–d), consistent with fractionation of olivine/pyroxene. The sharp rise in Dy/Yb ratios and δ^{57}Fe values at ~48 wt.% SiO_2 may result from garnet fractionation, which concentrates significant Yb and much light Fe isotopes due to its large proportion of ferrous iron and high coordination number (Jenner et al., 1993; Sossi and O'Neill, 2017). Increase of H_2O contents promotes amphibole saturation during magma evolution and emplacement. The Dy/Yb ratios and δ^{57}Fe values dramatically fall at ~51 wt.% SiO_2, reflecting large amounts of amphibole removal (Fig. 7a–d). Similar correlations are also clearly observed in plots of SiO_2 and MgO against δ^{56}Fe (Fig. 7e and f). The Fe isotope variations can be well modeled by fractional crystallization using $\Delta^{57}Fe_{mineral\text{-}melt} = -0.25$ to +0.20‰ and $\Delta^{56}Fe_{mineral\text{-}melt} = -0.17$ to +0.14‰ (Fig. 7c-f), the similar fractionation factors have been used in the Kilauea Iki Lava Lake (Teng et al., 2008), Hekla volcano

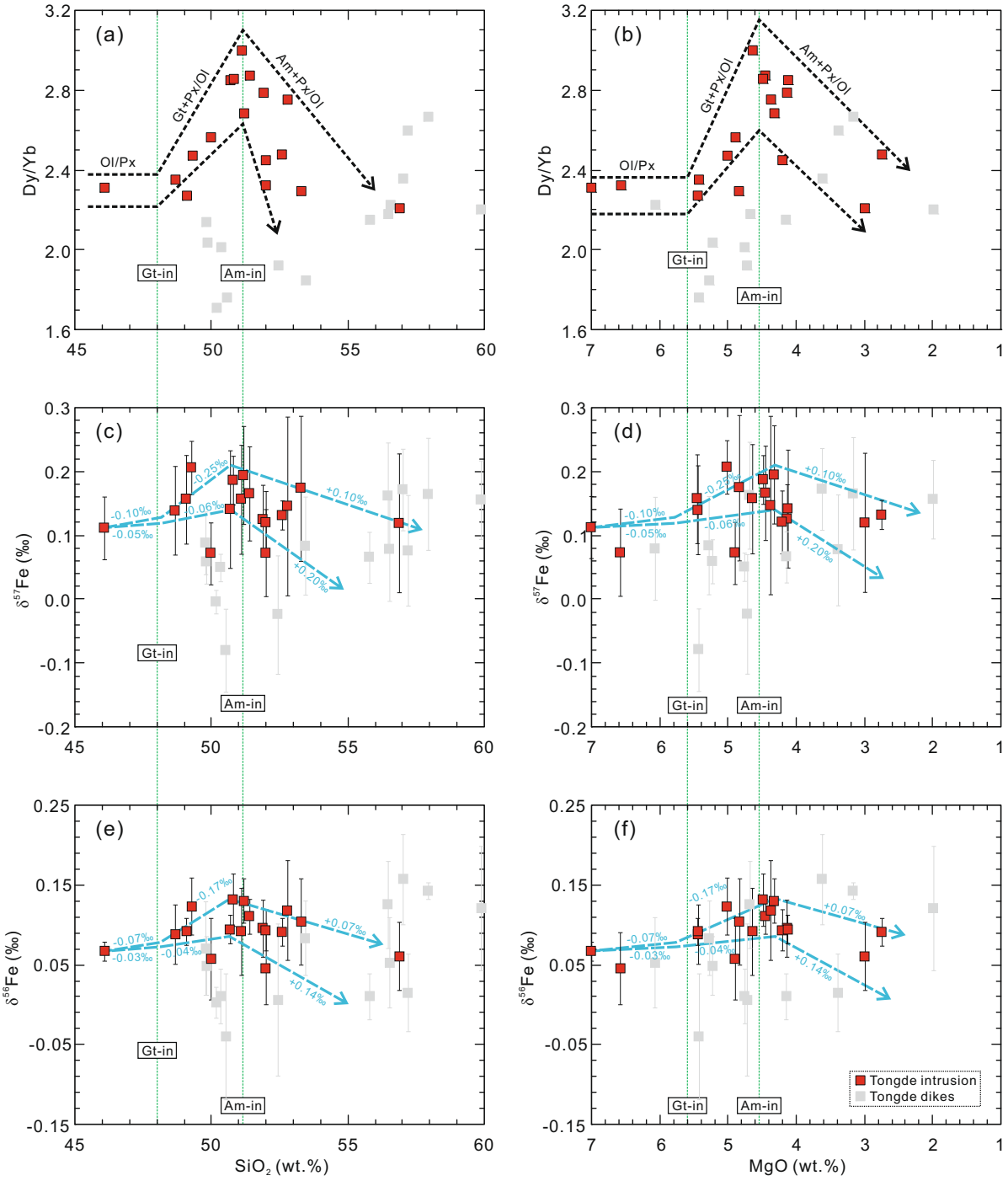

Fig. 7. Plots of Dy/Yb, $\delta^{57}Fe$ and $\delta^{56}Fe$ against SiO_2 and MgO for rocks from the Tongde intrusion and dikes. Vertical dashed lines indicate garnet-in (Gt-in) at ~48 wt.% SiO_2 and ~5.6 wt.% MgO, and amphibole-in (Am-in) at ~51 wt.% SiO_2 and ~4.6 wt.% MgO. Arrows in panels (a) and (b) show the Dy/Yb variation trends with the magma differentiation. The curves in panels (c) to (f) show Fe isotope compositions of residual melts with fractionation factors ($\Delta^{57}Fe_{mineral\text{-}melt}$) of −0.25 to +0.20‰. Major element variations were conducted by Rhyolite-MELTS modeling that started from sample TD36. $\Delta^{56}Fe_{mineral\text{-}melt}$ is derived from $\Delta^{57}Fe_{mineral\text{-}melt}$ using the theoretical mass dependent fractionation of 0.678 (Sossi and O'Neill, 2017).

(Schuessler et al., 2009) and Red Hill intrusion (Sossi et al., 2012). Apparent sources of uncertainty in the calculations are the Fe isotope fractionation factors, which vary significantly with variable Fe-O force constants (e.g., 133 vs 197 N/m in olivine, 108 vs 195–165 N/m in pyroxene, 147 vs 111 N/m in garnet; Polyakov and Mineev, 2000; Jackson et al., 2009; Dauphas et al., 2014; Sossi and O'Neill, 2017). $\delta^{57}Fe$ lacks correlations with FeO_t and Eu/Eu*, ruling out significant effects of magnetite fractionation and plagioclase accumulation on the Fe isotope variations

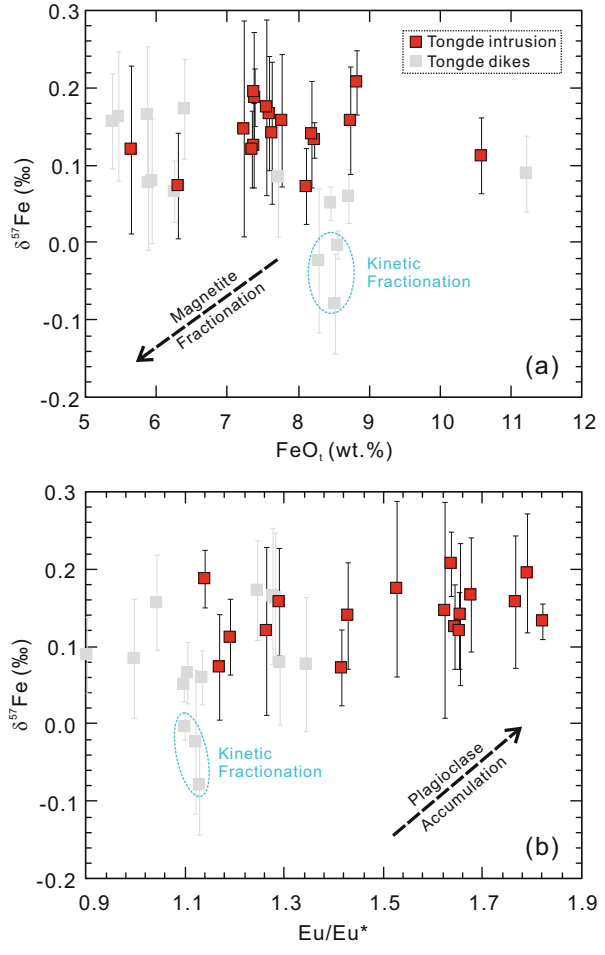

Fig. 8. Plots of FeO_t and Eu/Eu* against $\delta^{57}Fe$ for rocks from the Tongde intrusion and dikes.

(Fig. 8; Wu et al., 2017). Therefore, rocks from the Tongde intrusion underwent fractional crystallization of olivine/pyroxene and garnet in the deep crust, and amphibole separation in the upper section.

To further address the fractionation process, Rayleigh modeling was conducted based on the above magma differentiation:

$$\delta^{57}Fe_{melt} = \left(\delta^{57}Fe_{initial} + 1000\right) \times f^{(\alpha-1)} - 1000 \quad (6)$$

where α is Fe isotope fractionation factor between mineral and melt derived from:

$$1000\ln\alpha_{mineral-melt} \approx \Delta^{57}Fe_{mineral-melt} = 4284 \times \frac{[F_{mineral} - F_{melt}]}{T^2} \quad (7)$$

The mass fraction of iron in the residual melt (f) is:

$$f = F'_{melt} \times \frac{C_{melt}}{C_{initial}} \quad (8)$$

where F'_{melt} is the mass fraction of residual melt, C_{melt} is the melt iron content and $C_{initial}$ is the initial iron abundance. Compared with NRIXS, conventional Mössbauer spectroscopy is more susceptible to systematic errors and the data are probably systematically underestimated (Dauphas et al., 2014; Roskosz et al., 2015). In this study, Fe-O force constants measured by NRIXS were applied to olivine and pyroxene (average of 196 N/m; Jackson et al., 2009; Dauphas et al., 2014), and those of garnet were calculated with ionicity of 0.47 and 0.36 (111 and 147 N/m; Sossi and O'Neill, 2017). Amphibole force constant is rarely measured or calculated due to its complicated crystal structures and chemical compositions (Leake et al., 1997), but can be estimated by the correlation with coordination number at a given ferric iron fraction (Sossi and O'Neill, 2017). Fe^{3+} and Fe^{2+} are in 6-fold and 6 to 8-fold coordination in amphibole, respectively (Shimizu et al., 2017). Rocks from the Tongde intrusion have amphiboles that consist of magnesiohornblende and tschermakite with $Fe^{3+}/\sum Fe$ ratios of 0.22–0.89 (Table S4; Sun, 2009), which yield high force constants (up to 300 N/m) that meet requirement of positive fractionation factors in the later stage of magma evolution (Fig. 7c-f). However, amphibole has a force constant of ~250 N/m if an average $Fe^{3+}/\sum Fe$ ratio of 0.53 and coordination number of 6–7 were used in the calculations. The fractional crystallization is estimated to be started at ~1150 °C according to clinopyroxene thermometer in the Tongde intrusion (Table S3; Putirka, 2008), approximately matching the Rhyolite-MELTS modeling results (Fig. S2). All samples have high whole-rock $Fe^{3+}/\sum Fe$ ratios (0.25–0.39) and fO_2 of FMQ + 1.3 to FMQ + 2.3 using the amphibole oxybarometry (Tables S2 and S4; Ridolfi et al., 2010), and fall in the moderately oxidized fields (Fig. S3; Blevin, 2004). The estimated oxygen fugacity for their primary magma is ~FMQ + 1 based on the correlations of ΔFMQ against SiO_2 and MgO of the rocks (Fig. S4), similar to fO_2 of arc magmas (e.g., Evans et al., 2012). Sample TD36 has the lowest SiO_2 (46.10 wt.%) and highest MgO (7.00 wt.%) and thus is chosen as the starting composition, which yields a force constant of 230 N/m (Dauphas et al., 2014). The calculated mineral-melt fractionation factors are $\Delta^{57}Fe_{gt\text{-}melt} = -0.25‰$ or −0.18‰, $\Delta^{57}Fe_{ol/px\text{-}melt} = -0.07‰$ and $\Delta^{57}Fe_{am\text{-}melt} = +0.04‰$ (Table 2), similar to the reported values in the previous studies (Beard and Johnson, 2004; Schoenberg et al., 2009; Williams et al., 2009; Sossi et al., 2012). Besides, Ye et al. (2020) derived the temperature-dependent equilibrium Fe isotope fractionation factors between amphibole and garnet by $1000\ln\alpha_{am-gt} = 0.33(\pm0.15) \times 10^6/T^2$, yielding similar $\Delta^{57}Fe_{am\text{-}gt}$ of +0.09 to +0.24‰. A series of mineral assemblages, including olivine/pyroxene, garnet + pyroxene/olivine, and amphibole + garnet + pyroxene/olivine, were modeled to constrain their effects on Fe isotope fractionation. Results show that the Fe isotope variations for rocks from the Tongde intrusion can be reproduced by sequential fractional crystallization of olivine/pyroxene and garnet in the deep crust followed by amphibole saturation in the upper section (Fig. 9).

5.4. Diffusion between molten dikes and solid intrusion

Diffusion generally occurs between co-existing minerals and melts (e.g., Dauphas et al., 2010; Teng et al., 2011; Sio et al., 2013; Oeser et al., 2015), and at the boundaries between melts and country rocks (e.g., Richter et al.,

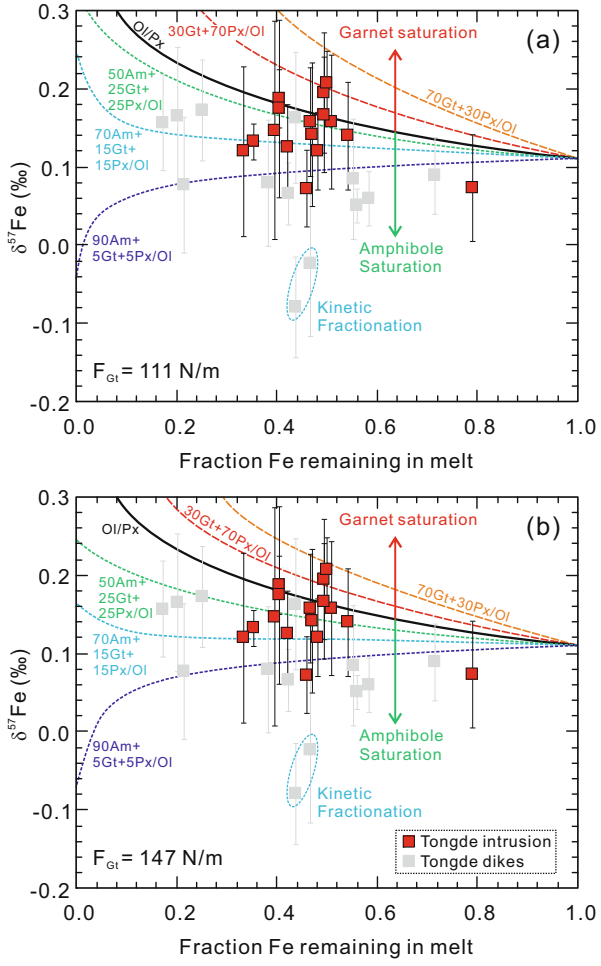

Fig. 9. Rayleigh fractionation modeling results show the Fe isotope variations in the residual melts during fractional crystallization of olivine/pyroxene, garnet and amphibole based on the garnet Fe-O force constants of 111 N/m (a) and 147 N/m (b).

2008, 2009; Wu et al., 2018), and will result in enrichment of light Fe isotopes and increasing Fe contents in the low-Fe side (Richter et al., 2003; Weyer and Ionov, 2007). The Tongde intrusion was formed ~10 Ma earlier than the dikes. Most samples from them have similar Fe isotopes, except that three ones from the dikes display much light δ^{57}Fe values and high FeO_t contents (Fig. 8a), that may have resulted from diffusive exchange (e.g., Wu et al., 2018).

The light δ^{57}Fe values can be fitted by self-diffusion of Fe between a molten dike and a solid intrusion. The one-dimensional diffusion model was used to model diffusion in two phases with different diffusivities. The interface between the intrusion and dike was set as $x = 0$; the initial effective element content (activity) at $x < 0$ (intrusion) is C_I, and at $x > 0$ (dike) is C_D. Fe has the self-diffusion coefficient D_I in the intrusion and D_D in the dike. The diffusion equation is written as (Zhang, 2008):

$$\frac{\partial C}{\partial t} = D\frac{\partial^2 C}{\partial x^2} \tag{9}$$

The initial condition is:

$$C_{t=0} = \begin{cases} C_I|x < 0 \\ C_D|x > 0 \end{cases} \tag{10}$$

The boundary condition is:

$$\frac{C_D}{C_I}_{x=0} = K \tag{11}$$

$$D_I\frac{\partial C_I}{\partial x}_{x=-0} = D_D\frac{\partial C_D}{\partial x}_{x=+0} \tag{12}$$

The solution of the diffusion equation can be obtained by:

$$C = C_I + \frac{C_D - KC_I}{K + \sqrt{D_I/D_D}}\,\mathrm{erfc}\frac{|x|}{2\sqrt{\int_0^t D_I dt}}, \quad \text{when } x < 0 \tag{13}$$

$$C = C_D + \frac{KC_I - C_D}{1 + K\sqrt{D_D/D_I}}\,\mathrm{erfc}\frac{x}{2\sqrt{\int_0^t D_D dt}}, \quad \text{when } x > 0 \tag{14}$$

where t is the diffusion duration, erfc is Gaussian error function, and diffusivity in the dike (D_D) was assumed to be ~2 times that of the intrusion (D_I). C_D and C_I are represented by relatively primitive samples TDM12 (SiO_2 = 56.55 wt.%, FeO_t = 5.94 wt.%, δ^{57}Fe = +0.08‰) and TD36 (SiO_2 = 46.10 wt.%, FeO_t = 10.59 wt.%, δ^{57}Fe = +0.11‰) (Tables 1 and S2; Li et al., 2020), respectively. The partition coefficient (K) of Fe between the melt and solid is estimated by the Fe content ratio of basaltic-andesitic melt to coexisting pyroxene that is ~1.5 in experimental melt at 55 wt.% SiO_2 (Nicholls and Harris, 1980; Dunn and Sen, 1994). ^{54}Fe and ^{57}Fe were treated as individual elements, and their diffusivity ratio was given by $D_{54}/D_{57} = (m_{57}/m_{54})^{\beta}$ (Richter et al., 1999), in which m_{57} and m_{54} are atomic masses of ^{57}Fe (56.935392) and ^{54}Fe (53.939608), respectively. $\beta = 0.08$ in this study is slightly higher than the experimental result (0.03 ± 0.01; Richter

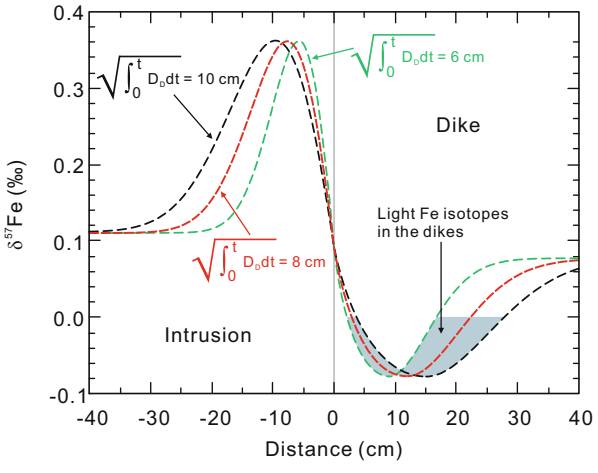

Fig. 10. Calculated Fe isotopic diffusion profile. Distance is given relative to the interface between the dike and intrusion. The diffusive transport distance ($\sqrt{\int_0^t D_D dt}$) is estimated to be 6, 8 and 10 cm to fit the light Fe isotope compositions of the dikes.

et al., 2009), probably because of different whole-rock chemical compositions from the experiment materials (e.g., Wu et al., 2018). Calculations reveal that the light Fe isotopes in the dikes could be generated through diffusion within 30 cm away from the interface (Fig. 10).

5.5. Implications for Fe isotope fractionation in basaltic and andesitic rocks and arc crustal evolution

The Tongde intrusion and dikes were emplaced in an arc setting at the western margin of the Yangtze Block (Zhao et al., 2011, 2018). These rocks were derived from a peridotite mantle source and evolved in deep crustal hot zones. Most samples have high Sr (411–1137 ppm) and low Y concentrations (7–21 ppm) and high Sr/Y ratios (33–163) (Table S2). Partial melting of a garnet-bearing lherzolite mantle cannot reproduce the primary Fe isotope compositions of the intrusion (Fig. 6b), whereas Rayleigh fractionation of olivine/pyroxene, garnet and amphibole allows Fe isotopes to evolve along a continuous liquid line of descent (Figs. 7 and 9). In combination with the Mesozoic-Cenozoic adakites (He et al., 2017), high Sr/Y samples with SiO_2 less than 65 wt.% show homogeneous Fe isotope compositions, similar to those of igneous rocks worldwide which are not significantly fractionated until SiO_2 contents above 65–70 wt.% (Fig. 11; Sossi et al., 2016; Du et al., 2017). We suggest that the small Fe isotope fractionation in low-Si igneous rocks can be well explained by fractionation of both isotopically light (e.g., olivine, pyroxene and garnet) and heavy minerals (e.g., amphibole), such a process may neutralize the possible Fe isotope variations in basaltic and andesitic rocks. It is thus possible to establish an average Fe isotope composition for high-Sr/Y rocks to evaluate contribution of garnet in deep crustal hot zones; rocks from the Tongde intrusion and dikes (excluding diffusion-affected samples) display δ^{57}Fe values ranging from +0.05‰ to +0.21‰ with an average of +0.11 ± 0.02‰ (2SD, n = 27). This value is similar to the average of arc crust at convergent continental margins (δ^{57}Fe = +0.13 ± 0.02‰, 2SD; Li et al., 2019), which is generally calc-alkaline in composition (Farner and Lee, 2017). Therefore, there is a possible link between garnet fractionation and crustal formation in arc roots, driving the melts to evolve to calc-alkaline series (e.g., Alonso-Perez et al., 2009). Fractional crystallization of hydrous basaltic magmas under high pressures in deep crustal hot zones makes a significant contribution to formation and evolution of the continental crust (Chin et al., 2018). Fe isotopes have the potential to trace the role of garnet in the above processes (Green, 1972; Alonso-Perez et al., 2009; Tang et al., 2018).

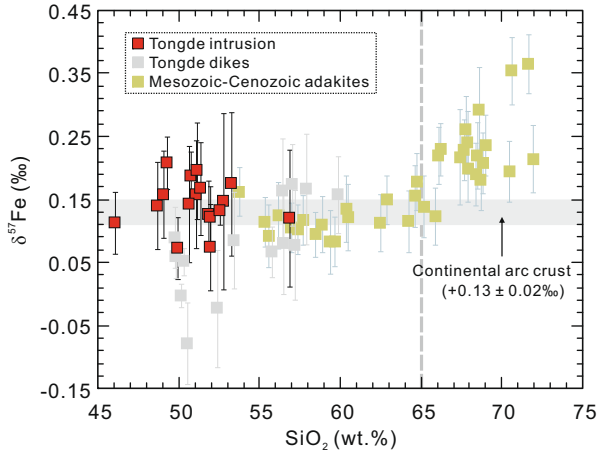

Fig. 11. Plot of δ^{57}Fe vs. SiO_2 for rocks from the Tongde intrusion and dikes. Mesozoic-Cenozoic adakites (He et al., 2017) and continental arc crust fields (Li et al., 2019) are shown for comparison.

6. CONCLUSIONS

The Fe isotope compositions of rocks from the Tongde intrusion lie within the previously reported range of global mafic and intermediate rocks, and show no imprint of fluid exsolution. Although all samples have high Sr/Y and $(La/Yb)_N$ ratios, partial melting of a garnet-bearing mantle source cannot reproduce the Fe isotope signatures of the primary melts. Instead, sequential fractional crystallization of olivine/pyroxene and garnet in the deep crust followed by amphibole saturation in the upper section is responsible for the observed Fe isotope variations. The host intrusion underwent diffusive exchange with the dikes. The small Fe isotope fractionation in low-Si igneous rocks can be well explained by fractional crystallization of various minerals. Removal of both isotopically light- and heavy-Fe phases may neutralize the possible Fe isotope variations in basaltic and andesitic rocks. The average δ^{57}Fe value of +0.11 ± 0.02‰ (2SD) for high-Sr/Y rocks in deep crustal hot zones is consistent with that reported for arc crust at convergent continental margins, suggesting a significant contribution of garnet fractionation in formation of calc-alkaline series rocks. Fe isotopes can be used as indicators in tracing the role of garnet in formation and evolution of continental crust.

Declaration of Competing Interest

The authors declare that they have no known competing financial interests or personal relationships that could have appeared to influence the work reported in this paper.

ACKNOWLEDGMENTS

This work was supported by the National Key R & D Program of China (No. 2016YFC0600407), the National Natural Science Foundation of China (Nos. 41773027, 41630208 and 91855215), the Key Program of the Chinese Academy of Sciences (QYZDJ-SSW-DQC026) and the China Postdoctoral Science Foundation (2018M643219). Dr. Wei-Hua Sun is thanked for his kind provision of some samples of the Tongde intrusion. We thank three anonymous reviewers for constructive comments and Stefan Weyer for editorial handling.

APPENDIX A. SUPPLEMENTARY MATERIAL

Supplementary data to this article can be found online at https://doi.org/10.1016/j.gca.2020.03.032.

REFERENCES

Alonso-Perez R., Müntener O. and Ulmer P. (2009) Igneous garnet and amphibole fractionation in the roots of island arcs: experimental constraints on andesitic liquids. *Contrib. Mineral. Petrol.* **157**, 541–558.

An Y., Huang J. X., Griffin W. L., Liu C. and Huang F. (2017) Isotopic composition of Mg and Fe in garnet peridotites from the Kaapvaal and Siberian cratons. *Geochim. Cosmochim. Acta* **200**, 167–185.

Annen C., Blundy J. D. and Sparks R. S. J. (2006) The genesis of intermediate and silicic magmas in deep crustal hot zones. *J. Petrol.* **47**, 505–539.

Anderson, Jr, A. T. (1979) Water in some hypersthenic magmas. *J. Geol.* **87**, 509–531.

Baker D. R. and Alletti M. (2012) Fluid saturation and volatile partitioning between melts and hydrous fluids in crustal magmatic systems: The contribution of experimental measurements and solubility models. *Earth Sci. Rev.* **114**, 298–324.

Barclay J. and Carmichael I. S. E. (2004) A hornblende basalt from western Mexico: water-saturated phase relations constrain a pressure-temperature window of eruptibility. *J. Petrol.* **45**, 485–506.

Bau M. (1996) Controls on the fractionation of isovalent trace elements in magmatic and aqueous systems: evidence from Y/Ho, Zr/Hf, and lanthanide tetrad effect. *Contrib. Mineral. Petrol.* **123**, 323–333.

Beard B. L. and Johnson C. M. (2004) Inter-mineral Fe isotope variations in mantle-derived rocks and implications for the Fe geochemical cycle. *Geochim. Cosmochim. Acta* **68**, 4727–4743.

Blevin P. L. (2004) Redox and compositional parameters for interpreting the granitoid metallogeny of eastern Australia: Implications for gold-rich ore systems. *Resour. Geol.* **54**, 241–252.

Castillo P. R. (2012) Adakite petrogenesis. *Lithos* **134**, 304–316.

Carmichael I. S. (2002) The andesite aqueduct: perspectives on the evolution of intermediate magmatism in west-central (105–99 W) Mexico. *Contrib. Mineral. Petrol.* **143**, 641–663.

Carmichael I. S. (2004) The activity of silica, water, and the equilibration of intermediate and silicic magmas. *Am. Mineral.* **89**, 1438–1446.

Candela P. A. (1986) The evolution of aqueous vapor from silicate melts: Effect on oxygen fugacity. *Geochim. Cosmochim. Acta* **50**, 1205–1211.

Canil D., O'Neill H. S. C., Pearson D. G., Rudnick R. L., McDonough W. F. and Carswell D. A. (1994) Ferric iron in peridotites and mantle oxidation states. *Earth Planet. Sci. Lett.* **123**, 205–220.

Cervantes P. and Wallace P. J. (2003) Role of H_2O in subduction-zone magmatism: new insights from melt inclusions in high-Mg basalts from central Mexico. *Geology* **31**, 235–238.

Chiaradia M., Müntener O., Beate B. and Fontignie D. (2009) Adakite-like volcanism of Ecuador: lower crust magmatic evolution and recycling. *Contrib. Mineral. Petrol.* **158**, 563–588.

Chin E. J., Shimizu K., Bybee G. M. and Erdman M. E. (2018) On the development of the calc-alkaline and tholeiitic magma series: A deep crustal cumulate perspective. *Earth Planet. Sci. Lett.* **482**, 277–287.

Chou I. M. and Eugster H. P. (1977) Solubility of magnetite in supercritical chloride solutions. *Am. J. Sci.* **277**, 1296–1314.

Craddock P. R. and Dauphas N. (2011) Iron isotopic compositions of geological reference materials and chondrites. *Geostand. Geoanal. Res.* **35**, 101–123.

Dalou C., Koga K. T., Shimizu N., Boulon J. and Devidal J. L. (2012) Experimental determination of F and Cl partitioning between lherzolite and basaltic melt. *Contrib. Mineral. Petrol.* **163**, 591–609.

Dauphas N., Craddock P. R., Asimow P. D., Bennett V. C., Nutman A. P. and Ohnenstetter D. (2009) Iron isotopes may reveal the redox conditions of mantle melting from Archean to Present. *Earth Planet. Sci. Lett.* **288**, 255–267.

Dauphas N., Teng F. Z. and Arndt N. T. (2010) Magnesium and iron isotopes in 2.7 Ga Alexo komatiites: Mantle signatures, no evidence for Soret diffusion, and identification of diffusive transport in zoned olivine. *Geochim. Cosmochim. Acta* **74**, 3274–3291.

Dauphas N., Roskosz M., Alp E. E., Neuville D. R., Hu M. Y., Sio C. K., Tissot F. L. H., Zhao J., Tissandier L., Médard E. and Cordier C. (2014) Magma redox and structural controls on iron isotope variations in Earth's mantle and crust. *Earth Planet. Sci. Lett.* **398**, 127–140.

Davidson J., Turner S., Handley H., Macpherson C. and Dosseto A. (2007) Amphibole 'sponge' in arc crust? *Geology* **35**, 787–790.

Defant M. J. and Drummond M. S. (1990) Derivation of some modern arc magmas by melting of young subducted lithosphere. *Nature* **347**, 662–665.

Dessimoz M., Müntener O. and Ulmer P. (2012) A case for hornblende dominated fractionation of arc magmas: the Chelan Complex (Washington Cascades). *Contrib. Mineral. Petrol.* **163**, 567–589.

Du D. H., Wang X. L., Yang T., Chen X., Li J. Y. and Li W. (2017) Origin of heavy Fe isotope compositions in high-silica igneous rocks: a rhyolite perspective. *Geochim. Cosmochim. Acta* **218**, 58–72.

Dunn T. and Sen C. (1994) Mineral/matrix partition coefficients for orthopyroxene, plagioclase, and olivine in basaltic to andesitic systems: a combined analytical and experimental study. *Geochim. Cosmochim. Acta* **58**, 717–733.

Evans K. A., Elburg M. A. and Kamenetsky V. S. (2012) Oxidation state of subarc mantle. *Geology* **40**, 783–786.

Farner M. J. and Lee C. T. A. (2017) Effects of crustal thickness on magmatic differentiation in subduction zone volcanism: a global study. *Earth Planet. Sci. Lett.* **470**, 96–107.

Foden J., Sossi P. A. and Wawryk C. M. (2015) Fe isotopes and the contrasting petrogenesis of A-, I- and S-type granite. *Lithos* **212**, 32–44.

Foden J., Sossi P. A. and Nebel O. (2018) Controls on the iron isotopic composition of global arc magmas. *Earth Planet. Sci. Lett.* **494**, 190–201.

Gaetani G. A., Kent A. J., Grove T. L., Hutcheon I. D. and Stolper E. M. (2003) Mineral/melt partitioning of trace elements during hydrous peridotite partial melting. *Contrib. Mineral. Petrol.* **145**, 391–405.

Gajos N. A., Lundstrom C. C. and Taylor A. H. (2016) Spatially controlled Fe and Si isotope variations: an alternative view on the formation of the Torres del Paine pluton. *Contrib. Mineral. Petrol.* **171**, 93.

Green T. H. (1972) Crystallization of calc-alkaline andesite under controlled high-pressure hydrous conditions. *Contrib. Mineral. Petrol.* **34**, 150–166.

Grove T. L., Elkins-Tanton L. T., Parman S. W., Chatterjee N., Müntener O. and Gaetani G. A. (2003) Fractional crystallization and mantle-melting controls on calc-alkaline differentiation trends. *Contrib. Mineral. Petrol.* **145**, 515–533.

Gualda G. A., Ghiorso M. S., Lemons R. V. and Carley T. L. (2012) Rhyolite-MELTS: a modified calibration of MELTS optimized for silica-rich, fluid-bearing magmatic systems. *J. Petrol.* **53**, 875–890.

Hawkesworth C. J., Turner S. P., McDermott F., Peate D. W. and van Calsteren P. (1997) U-Th isotopes in arc magmas: implications for element transfer from the subducted crust. *Science* **276**, 551–555.

He Y., Ke S., Teng F. Z., Wang T., Wu H., Lu Y. and Li S. (2015) High-precision iron isotope analysis of geological reference materials by high-resolution MC-ICP-MS. *Geostand. Geoanal. Res.* **39**, 341–356.

He Y., Wu H., Ke S., Liu S. A. and Wang Q. (2017) Iron isotopic compositions of adakitic and non-adakitic granitic magmas: Magma compositional control and subtle residual garnet effect. *Geochim. Cosmochim. Acta* **203**, 89–102.

Heimann A., Beard B. L. and Johnson C. M. (2008) The role of volatile exsolutions and sub-solidus fluid/rock interactions in producing high $^{56}Fe/^{54}Fe$ ratios in siliceous igneous rocks. *Geochim. Cosmochim. Acta* **72**, 4379–4396.

Hoffer G., Eissen J. P., Beate B., Bourdon E., Fornari M. and Cotten J. (2008) Geochemical and petrological constraints on rear-arc magma genesis processes in Ecuador: the Puyo cones and Mera lavas volcanic formations. *J. Volcanol. Geotherm. Res.* **176**, 107–118.

Huang F., Lundstrom C. C., Glessner J., Ianno A., Boudreau A., Li J., Ferré E. C., Marshak S. and DeFrates J. (2009) Chemical and isotopic fractionation of wet andesite in a temperature gradient: experiments and models suggesting a new mechanism of magma differentiation. *Geochim. Cosmochim. Acta* **73**, 729–749.

Jackson J. M., Hamecher E. A. and Sturhahn W. (2009) Nuclear resonant X-ray spectroscopy of (Mg, Fe)SiO_3 orthoenstatites. *Eur. J. Mineral.* **21**, 551–560.

Jagoutz O., Muntener O., Ulmer P., Pettke T., Burg J. P., Dawood H. and Hussain S. (2007) Petrology and mineral chemistry of lower crustal intrusions: the Chilas Complex, Kohistan (NW Pakistan). *J. Petrol.* **48**, 1895–1953.

Jenner G. A., Foley S. F., Jackson S. E., Green T. H., Fryer B. J. and Longerich H. P. (1993) Determination of partition coefficients for trace elements in high pressure-temperature experimental run products by laser ablation microprobe-inductively coupled plasma-mass spectrometry (LAM-ICP-MS). *Geochim. Cosmochim. Acta* **57**, 5099–5103.

Kelley K. A. and Cottrell E. (2009) Water and the oxidation state of subduction zone magmas. *Science* **325**, 605–607.

Klaver M., Blundy J. D. and Vroon P. Z. (2018) Generation of arc rhyodacites through cumulate-melt reactions in a deep crustal hot zone: Evidence from Nisyros volcano. *Earth Planet. Sci. Lett.* **497**, 169–180.

Kolb M., Von Quadt A., Peytcheva I., Heinrich C. A., Fowler S. J. and Cvetković V. (2012) Adakite-like and normal arc magmas: distinct fractionation paths in the East Serbian segment of the Balkan-Carpathian arc. *J. Petrol.* **54**, 421–451.

Leake B. E., Woolley A. R., Arps C. E. S., Birch W. D., Gilbert M. C., Grice J. D., Hawthorne F. C., Kato A., Kisch H. J., Krivovichev V. G., Linthout K., Laird J., Mandarino J. A., Maresch W. V., Nickel E. H., Rock N. M. S., Schumacher J. C., Smith D. C., Stephenson N. C. N., Ungaretti L., Whittaker E. J. W. and Guo Y. Z. (1997) Nomenclature of amphiboles: report of the subcommittee on amphiboles of the international mineralogical association, commission on new minerals and mineral names. *Am. Mineral.* **82**, 1019–1037.

Li Q. W. and Zhao J. H. (2018) The Neoproterozoic high-Mg dioritic dikes in South China formed by high pressures fractional crystallization of hydrous basaltic melts. *Precambrian Res.* **309**, 198–211.

Li Q. W., Nebel O., Nebel-Jacobsen Y., Richter M., Wang R., Weinberg R., Zhao J. H. and Cawood P. A. (2019) Crustal reworking at convergent margins traced by Fe isotopes in I-type intrusions from the Gangdese arc, Tibetan Plateau. *Chem. Geol.* **510**, 47–55.

Li Q. W., Nebel O., Zhao J. H., Nebel-Jacobsen Y., Richter M., Cawood P. A. and Wang Q. (2020) An early garnet redox-filter in lower crustal arc zones traced through Fe isotopes (in review).

Macpherson C. G., Dreher S. T. and Thirlwall M. F. (2006) Adakites without slab melting: high pressure differentiation of island arc magma, Mindanao, the Philippines. *Earth Planet. Sci. Lett.* **243**, 581–593.

Moyen J. F. (2009) High Sr/Y and La/Yb ratios: the meaning of the "adakitic signature". *Lithos* **112**, 556–574.

Müntener O. and Ulmer P. (2006) Experimentally derived high-pressure cumulates from hydrous arc magmas and consequences for the seismic velocity structure of lower arc crust. *Geophys. Res. Lett.* **33**, L21308.

Nebel O., Sossi P. A., Benard A., Wille M., Vroon P. Z. and Arculus R. J. (2015) Redox variability and controls in subduction zones from an iron-isotope perspective. *Earth Planet. Sci. Lett.* **432**, 142–151.

Nebel O., Sossi P. A., Foden J., Bénard A., Brandl P. A., Stammeier J. A., Lupton J., Richter M. and Arculus R. J. (2018) Iron isotope variability in ocean floor lavas and mantle sources in the Lau back-arc basin. *Geochim. Cosmochim. Acta* **241**, 150–163.

Nicholls I. A. and Harris K. L. (1980) Experimental rare earth element partition coefficients for garnet, clinopyroxene and amphibole coexisting with andesitic and basaltic liquids. *Geochim. Cosmochim. Acta* **44**, 287–308.

Oeser M., Dohmen R., Horn I., Schuth S. and Weyer S. (2015) Processes and time scales of magmatic evolution as revealed by Fe-Mg chemical and isotopic zoning in natural olivines. *Geochim. Cosmochim. Acta* **154**, 130–150.

Poitrasson F. and Freydier R. (2005) Heavy iron isotope composition of granites determined by high resolution MC-ICP-MS. *Chem. Geol.* **222**, 123–147.

Polyakov V. B. and Mineev S. D. (2000) The use of Mössbauer spectroscopy in stable isotope geochemistry. *Geochim. Cosmochim. Acta* **64**, 849–865.

Polyakov V. B., Clayton R. N., Horita J. and Mineev S. D. (2007) Equilibrium iron isotope fractionation factors of minerals: reevaluation from the data of nuclear inelastic resonant X-ray scattering and Mössbauer spectroscopy. *Geochim. Cosmochim. Acta* **71**, 3833–3846.

Putirka K. D. (2008) Thermometers and barometers for volcanic systems. In: Minerals, Inclusions and Volcanic Processes (eds. K. D. Putirka and F. J. Tepley III). Mineralogical Society of America and Geochemical Society, Rev. Mineral. Geochem. 69, 61–120.

Ribeiro J. M., Maury R. C. and Grégoire M. (2016) Are adakites slab melts or high-pressure fractionated mantle melts? *J. Petrol.* **57**, 839–862.

Richter F. M., Liang Y. and Davis A. M. (1999) Isotope fractionation by diffusion in molten oxides. *Geochim. Cosmochim. Acta* **63**, 2853–2861.

Richter F. M., Davis A. M., DePaolo D. J. and Watson E. B. (2003) Isotope fractionation by chemical diffusion between molten basalt and rhyolite. *Geochim. Cosmochim. Acta* **67**, 3905–3923.

Richter F. M., Watson E. B., Mendybaev R. A., Teng F. Z. and Janney P. E. (2008) Magnesium isotope fractionation in silicate

melts by chemical and thermal diffusion. *Geochim. Cosmochim. Acta* **72**, 206–220.
Richter F. M., Watson E. B., Mendybaev R., Dauphas N., Georg B., Watkins J. and Valley J. (2009) Isotopic fractionation of the major elements of molten basalt by chemical and thermal diffusion. *Geochim. Cosmochim. Acta* **73**, 4250–4263.
Ridolfi F., Renzulli A. and Puerini M. (2010) Stability and chemical equilibrium of amphibole in calc-alkaline magmas: an overview, new thermobarometric formulations and application to subduction-related volcanoes. *Contrib. Mineral. Petrol.* **160**, 45–66.
Roskosz M., Sio C. K., Dauphas N., Bi W., Tissot F. L., Hu M. Y., Zhao J. and Alp E. E. (2015) Spinel-olivine-pyroxene equilibrium iron isotopic fractionation and applications to natural peridotites. *Geochim. Cosmochim. Acta* **169**, 184–199.
Rudnick R. L. and Gao S. (2003) Composition of the continental crust. *Treatise Geochem.* **3**, 1–64.
Schoenberg R., Marks M. A., Schuessler J. A., von Blanckenburg F. and Markl G. (2009) Fe isotope systematics of coexisting amphibole and pyroxene in the alkaline igneous rock suite of the Ilímaussaq Complex, South Greenland. *Chem. Geol.* **258**, 65–77.
Schuessler J. A., Schoenberg R. and Sigmarsson O. (2009) Iron and lithium isotope systematics of the Hekla volcano, Iceland - evidence for Fe isotope fractionation during magma differentiation. *Chem. Geol.* **258**, 78–91.
Shaw D. M. (1970) Trace element fractionation during anatexis. *Geochim. Cosmochim. Acta* **34**, 237–243.
Shimizu K., Liang Y., Sun C., Jackson C. R. and Saal A. E. (2017) Parameterized lattice strain models for REE partitioning between amphibole and silicate melt. *Am. Mineral.* **102**, 2254–2267.
Simon A. C., Pettke T., Candela P. A., Piccoli P. M. and Heinrich C. A. (2004) Magnetite solubility and iron transport in magmatic-hydrothermal environments. *Geochim. Cosmochim. Acta* **68**, 4905–4914.
Sisson T. W. and Grove T. L. (1993) Experimental investigations of the role of H_2O in calc-alkaline differentiation and subduction zone magmatism. *Contrib. Mineral. Petrol.* **113**, 143–166.
Sio C. K. I., Dauphas N., Teng F. Z., Chaussidon M., Helz R. T. and Roskosz M. (2013) Discerning crystal growth from diffusion profiles in zoned olivine by in situ Mg-Fe isotopic analyses. *Geochim. Cosmochim. Acta* **123**, 302–321.
Solano J. M. S., Jackson M. D., Sparks R. S. J., Blundy J. D. and Annen C. (2012) Melt segregation in deep crustal hot zones: a mechanism for chemical differentiation, crustal assimilation and the formation of evolved magmas. *J. Petrol.* **53**, 1999–2026.
Sossi P. A., Foden J. D. and Halverson G. P. (2012) Redox controlled iron isotope fractionation during magmatic differentiation: an example from the Red Hill intrusion, S. Tasmania. *Contrib. Mineral. Petrol.* **164**, 757–772.
Sossi P. A., Nebel O. and Foden J. (2016) Iron isotope systematics in planetary reservoirs. *Earth Planet. Sci. Lett.* **452**, 295–308.
Sossi P. A. and O'Neill H. S. C. (2017) The effect of bonding environment on iron isotope fractionation between minerals at high temperature. *Geochim. Cosmochim. Acta* **196**, 121–143.
Sun W. H. (2009) *The Neoproterozoic Yanbian Group and Associated Plutons in the Western Yangtze block, SW China (Doctoral dissertation)*. The University of Hong Kong, Hong Kong, China.
Tang M., Erdman M., Eldridge G. and Lee C. T. A. (2018) The redox "filter" beneath magmatic orogens and the formation of continental crust. *Sci. Adv.* **4**, eaar4444.
Telus M., Dauphas N., Moynier F., Tissot F. L. H., Teng F. Z., Nabelek P. I. and Groat L. A. (2012) Iron, zinc, magnesium and uranium isotopic fractionation during continental crust differentiation: the tale from migmatites, granitoids, and pegmatites. *Geochim. Cosmochim. Acta* **97**, 247–265.
Teng F. Z., Dauphas N. and Helz R. T. (2008) Iron isotope fractionation during magmatic differentiation in Kilauea Iki Lava Lake. *Science* **320**, 1620–1622.
Teng F. Z., Dauphas N., Helz R. T., Gao S. and Huang S. (2011) Diffusion-driven magnesium and iron isotope fractionation in Hawaiian olivine. *Earth Planet. Sci. Lett.* **308**, 317–324.
Tiepolo M., Oberti R., Zanetti A., Vannucci R. and Foley S. F. (2007) Trace element partitioning between amphibole and silicate melt. In: Amphiboles: Crystal Chemistry, Occurrence, and Health Issues (eds. F. C. Hawthorne, R. Oberti, G. Della Ventura and A. Mottana). Mineralogical Society of America and Geochemical Society, Rev. Mineral. Geochem. 67, 417–452.
Walter M. J. (1998) Melting of garnet peridotite and the origin of komatiite and depleted lithosphere. *J. Petrol.* **39**, 29–60.
Weyer S. and Ionov D. A. (2007) Partial melting and melt percolation in the mantle: the message from Fe isotopes. *Earth Planet. Sci. Lett.* **259**, 119–133.
Weyer S. (2008) What drives iron isotope fractionation in magma? *Science* **320**, 1600–1601.
Williams H. M., Nielsen S. G., Renac C., Griffin W. L., O'Reilly S. Y., McCammon C. A., Pearson N., Viljoen F., Alt J. C. and Halliday A. N. (2009) Fractionation of oxygen and iron isotopes by partial melting processes: implications for the interpretation of stable isotope signatures in mafic rocks. *Earth Planet. Sci. Lett.* **283**, 156–166.
Williams H. M., Prytulak J., Woodhead J. D., Kelley K. A., Brounce M. and Plank T. (2018) Interplay of crystal fractionation, sulfide saturation and oxygen fugacity on the iron isotope composition of arc lavas: an example from the Marianas. *Geochim. Cosmochim. Acta* **226**, 224–243.
Workman R. K. and Hart S. R. (2005) Major and trace element composition of the depleted MORB mantle (DMM). *Earth Planet. Sci. Lett.* **231**, 53–72.
Wu H., He Y., Bao L., Zhu C. and Li S. (2017) Mineral composition control on inter-mineral iron isotopic fractionation in granitoids. *Geochim. Cosmochim. Acta* **198**, 208–217.
Wu H., He Y., Teng F. Z., Ke S., Hou Z. and Li S. (2018) Diffusion-driven magnesium and iron isotope fractionation at a gabbro-granite boundary. *Geochim. Cosmochim. Acta* **222**, 671–684.
Xia Y., Li S. and Huang F. (2017) Iron and Zinc isotope fractionation during magmatism in the continental crust: Evidence from bimodal volcanic rocks from Hailar basin, NE China. *Geochim. Cosmochim. Acta* **213**, 35–46.
Xu W., Zhu D. C., Wang Q., Weinberg R. F., Wang R., Li S. M., Zhang L. L. and Zhao Z. D. (2019) Constructing the Early Mesozoic Gangdese Crust in Southern Tibet by Hornblende-dominated Magmatic Differentiation. *J. Petrol.* **60**, 515–552.
Ye H., Wu C., Brzozowski M. J., Yang T., Zha X., Zhao S., Gao B. and Li W. (2020) Calibrating equilibrium Fe isotope fractionation factors between magnetite, garnet, amphibole, and biotite. *Geochim. Cosmochim. Acta* **271**, 78–95.
Zambardi T., Lundstrom C. C., Li X. and McCurry M. (2014) Fe and Si isotope variations at Cedar Butte volcano; insight into magmatic differentiation. *Earth Planet. Sci. Lett.* **405**, 169–179.
Zhang L., Sun W., Zhang Z., An Y. and Liu F. (2019) Iron isotopic composition of supra-subduction zone ophiolitic peridotites from northern Tibet. *Geochim. Cosmochim. Acta* **258**, 274–289.
Zhang Y. (2008) *Geochemical Kinetics*. Princeton University Press.
Zhao J. H., Zhou M. F., Yan D. P., Zheng J. P. and Li J. W. (2011) Reappraisal of the ages of Neoproterozoic strata in South China: no connection with the Grenvillian orogeny. *Geology* **39**, 299–302.

Zhao J. H. and Asimow P. D. (2018) Formation and evolution of a magmatic system in a rifting continental margin: Neoproterozoic arc- and MORB-like dike swarms in South China. *J. Petrol.* **59**, 1811–1844.

Zhao J. H., Li Q. W., Liu H. and Wang W. (2018) Neoproterozoic magmatism in the western and northern margins of the Yangtze Block (South China) controlled by slab subduction and subduction-transform-edge-propagator. *Earth Sci. Rev.* **187**, 1–18.

Zimmer M. M., Plank T., Hauri E. H., Yogodzinski G. M., Stelling P., Larsen J., Singer B., Jicha B., Mandeville C. and Nye C. J. (2010) The role of water in generating the calc-alkaline trend: new volatile data for Aleutian magmas and a new tholeiitic index. *J. Petrol.* **51**, 2411–2444.

Associate editor: Stefan Weyer